PHYSICAL REVIEW B

SOLID STATE

THIRD SERIES, VOL. 5, NO. 9 1 MAY 1972

Optical Properties of Fe^{3+} in Ordered and Disordered $LiAl_5O_8$ †

N. T. Melamed
Westinghouse Research Laboratories, Pittsburgh, Pennsylvania 15235

and

F. de S. Barros, * P. J. Viccaro, ‡ and J. O. Artman§
Department of Physics, Carnegie-Mellon University, Pittsburgh, Pennsylvania 15213

(Received 17 June 1971)

The fluorescence and excitation spectra of Fe^{3+} in the ordered and disordered phases of the spinel $LiAl_5O_8$ have been measured at 77 and 4.2 K. At these temperatures, a strong zero-phonon line is observed in the ordered-phase fluorescence accompanied by relatively well-defined vibronic sidebands. These sidebands are separated by a common frequency interval of 199 cm^{-1}. Their origin is attributed to local modes of an $[FeO_4]$ center. Several large splittings are observed. A splitting of approximately 600 cm^{-1} is seen in the $^4T_1(^4G)$ and $^4T_2(^4G)$ levels at the tetrahedral sites. A splitting of 16 cm^{-1} seen in the zero-phonon line is believed due to spin-orbit effects. Good agreement is obtained between calculated and observed level positions. Our earlier suggestion that the fluorescence of the ordered phase is due to Fe^{3+} at tetrahedral (A) sites while the fluorescence of the disordered phase is due to Fe^{3+} at octahedral (B) sites is strengthened. Finally, we present a comparison of certain basic features of $LiAl_5O_8:Fe^{3+}$ obtained from optical measurements with those obtained from Mössbauer-effect measurements. The latter will be published separately.

I. INTRODUCTION

$LiAl_5O_8$ is a synthetic mineral with a modified inverse-spinel structure. Fe^{3+}, when present in the $LiAl_5O_8$ matrix, exhibits interesting fluorescent and magnetic hyperfine properties. The magnetic hyperfine properties have been extensively studied by us by means of the Mössbauer effect (ME); these will be discussed in a future publication.[1] The room-temperature fluorescent properties of Fe^{3+} present in both the ordered and disordered $LiAl_5O_8$ phases had been described in an earlier publication,[2] hereafter referred to as MVAB-I. The present paper presents results of optical measurements taken at 77 and 4 K. An over-all interpretation of all the optical data is also given. In particular we (a) substantiate the Fe^{3+}-site occupancies derived from room-temperature data, (b) reconcile the observed positions of the energy levels with crystal field calculations, (c) account for the splittings observed in the ordered phase.

II. BACKGROUND

A. Crystallographic Properties

In the spinel structure, the cations occupy both tetrahedral and octahedral sites. These are located at the interstices of a close-packed oxygen lattice.[3] In the case of $LiAl_5O_8$, two stable crystalline phases are possible, depending on the formation temperature of the system. Below 1295 °C there exists a 1:3 ordering of the lithium and trivalent ions along the [110] directions of the unit cell.[4] In this ordered phase, each Li^+ ion is followed by three trivalent cations; both types of ions are octahedrally coordinated with oxygen (see Fig. 1). The primitive cell is primitive cubic, being characterized by the space group $P4_332(O^7)$ or the enantiomorph $P4_132(O^6)$. Above 1295 °C the 1:3 ordering is destroyed and the two types of cations are randomly distributed over the octahedral sites. The resulting phase is referred to as the disordered phase. By rapidly quenching the specimen from a high temperature, this phase can be retained indefinitely at room and lower temperatures. In this disordered or high-temperature phase the average structure is one of higher over-all symmetry; the space group corresponds to the standard spinel structure $Fd\bar{3}2m(O_h^7)$. The site symmetried of the trivalent cations in both phases are tabulated in Table I. Both phases contain four nonequivalent A sites

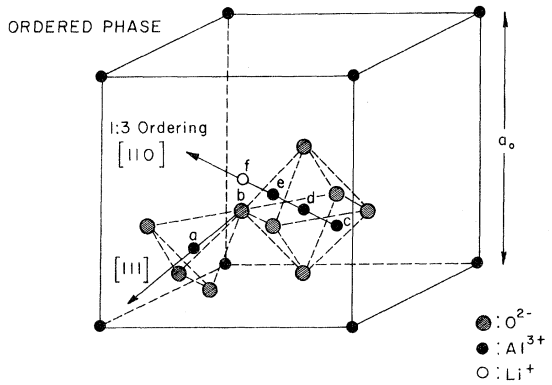

FIG. 1. Partial representation of the 1:3 ordered spinel $LiAl_5O_8$. Cation *a* lies at a tetrahedral site on a [111] line and is colinear with oxygen *b*. Cations *c*, *d*, *e*, and *f* are at octahedral sites. The 1:3 ordering of the octahedral Li^+ and Al^{3+} ions is along the [110] direction.

per unit cell and 12 nonequivalent *B* sites. The lattice parameters[4] of $LiAl_5O_8$ in the ordered and disordered phases are 7.907 and 7.921 Å, respectively.

To this point an ideal structure has been described. In reality, the aluminate deviates from this model somewhat. One such deviation concerns the Li^+- and Al^{3+}-site occupancy in both the high- and low-temperature phases and the actual degree of long-range order in the latter. In general, both phases can be written as $(Li_xAl_{2-x})^{IV}(Li_{1-x}Al_{3+x})^{VI}O_8$, where x indicates the fraction of improperly coordinated Li^+ ions on tetrahedral sites. Estimates[4,5] of this fraction x in the ordered phase from x-ray-diffraction intensities range from 0.13 to 0.33. (However, we see no evidence of such an improperly coordinated fraction in our Mössbauer-effect studies. We estimate our ME sensitivity to correspond to a value of $x \leq 0.05$.) Another type of deviation relates to the systematic distortion of the cubic oxygen sublattice. A measure of this distortion is the oxygen position parameter u, which for an ideal cubic-close-packed array of O^{2-} ions has the value of 0.375. For ordered $LiAl_5O_8$, u is found to be 0.385.[6]

A final interesting feature of $LiAl_5O_8$: Fe^{3+} is the relative site preferences of Al^{3+} and Fe^{3+}. Miller[7] has shown theoretically that the Al^{3+}: Fe^{3+} preference for octahedral-*B*-site occupation in spinels is, on the basis of binding energy, nearly 4:1. Experimentally, it has been shown[8] that the Al^{3+} in iron-rich ordered-phase aluminate-ferrite systems enters principally on the *B* sites.

TABLE I. Site symmetries of cations in ordered and disordered $LiAl_5O_8$.

Phase	*A* (tetrahedral) site symmetry	*B* (octahedral) site symmetry
Ordered	$3(C_3)$	$2(C_2)$
Disordered	$\bar{4}3m(T_d)$	$3m(D_{3d})$

B. Previous Luminescence Observations

As we previously reported,[2] at room temperature ordered $LiAl_5O_8$: Fe^{3+} fluoresces in a broad band with a maximum at about 680 nm (14 700 cm^{-1}) and a width at half-maximum of about 62.5 nm (1300 cm^{-1}); see Fig. 2(a). This band consists of two broad components which overlap significantly. The shorter-wavelength component (at 668.0 nm) has a decay constant of 6.2 msec; the longer-wavelength component (at 697.5 nm) has a decay constant of 1.72 msec. The excitation spectrum of the fluorescence consists of several distinct spectral bands. A sharp band at 390 nm (25 600 cm^{-1}) was easily identified as arising from the $^6A_1(^6S) \rightarrow {}^4A_1, {}^4E(^4G)$ transition of Fe^{3+}. A broader band, centered at 440 nm (22 700 cm^{-1}), was identified as arising from the $^6A_1(^6S) \rightarrow {}^4T_2(^4G)$ transition. This band also contains two clearly distinguishable

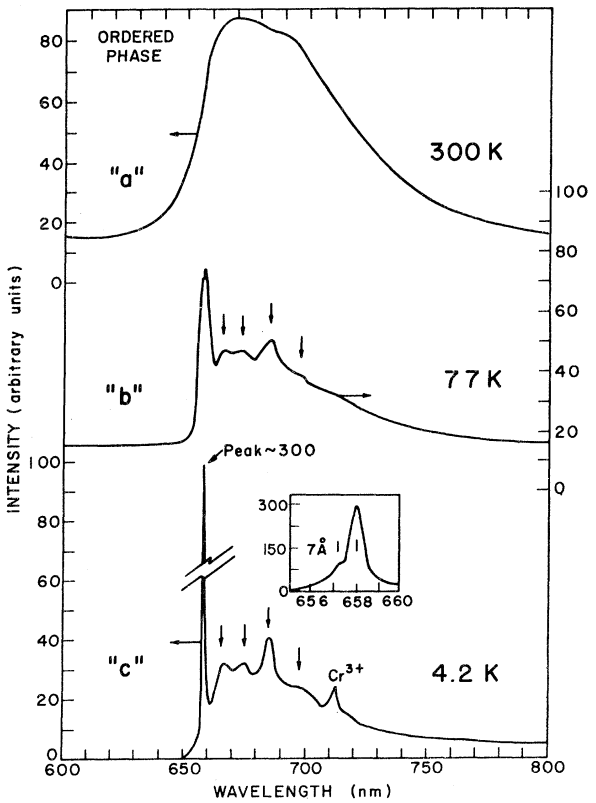

FIG. 2. Fluorescence of ordered $LiAl_5O_8$: Fe^{3+} at (a) 300 K, (b) 77 K, and (c) 4.2 K. The components of the zero-phonon line at 4.2 K are shown in the insert. The positions of the observed vibronic sidebands at 77 and 4.2 K are indicated by arrows.

components. Finally, a very weak band was observed centered at 520 nm (19 200 cm^{-1}). Its width appeared to be comparable to the fluorescence band.

The room-temperature fluorescence of the disordered phase, shown here in Fig. 6(a), differs from that of the ordered phase in several respects. It occurs at a significantly longer wavelength, 725 nm (13 800 cm^{-1}). There is no evidence of pronounced structure in this band. The excitation spectrum is similar to that of the ordered phase except for the absence of evidence of splitting in the observed bands; furthermore we could not detect any weak band at about 520 nm. This last aspect had an important influence on our interpretation of these disordered-phase spectra.

Based on the interpretations of ME,[1] EPR,[9] and to some extent of our previous spectroscopic data, we attributed the fluorescence of the ordered phase to Fe^{3+} ions situated at tetrahedral (A) sites, and the fluorescence of the disordered phase to Fe^{3+} situated at octahedral (B) sites. Two interpretations for the 520-nm ordered-phase band were suggested. The first assigned it to the $^6A_1(^6S) \rightarrow {}^4T_1(^4G)$ transition (the inverse of the emission process). Such an assignment presumed a very large Stokes shift of approximately 4500 cm^{-1}, or 35% of the fluorescent transition energy. A second interpretation attributed the 520-nm band to the $^6A_1(^6S) \rightarrow {}^2T_2(^2I)$ transition. The very low oscillator strength of this transition and its position in the spectrum qualitatively agreed with this assignment. Unfortunately, assignment of the 520-nm band to the $^2T_2(^2I) \rightarrow {}^6A(^6S)$ transition could not be reconciled with crystal field calculations, despite the use of various correction factors.[2]

III. EXPERIMENTAL PROCEDURES

The methods and apparatus used in these low-temperature investigations were for the most part similar to those used previously,[2] except for the method of mounting samples. For measurements at 4 and 77 K, the samples were packed into thin-walled fused-silica capillaries which were evacuated, filled with He at approximately 300 torr, and scaled. Excitation and fluorescence measurements at 77 K were obtained using our Excifluor,[2] with the sample capillary immersed in liquid N_2 contained in a small unsilvered Dewar of fused silica. For fluorescence measurements at 4.2 K, a Sulfrian liquid-He Dewar equipped with optical windows was used. The sample capillaries were immersed in liquid He. The fluorescence was analyzed by means of a 0.5-m JACO grating spectrometer equipped with an uncorrected S20 photomultiplier.

To obtain signal-averaged excitation spectra, a modification in the earlier procedure was required. This consisted of replacing the lock-in amplifier and recorder used in the signal-detection circuit with a Fabri-Tek-1062 multichannel signal averager. At the same time, the dc xenon lamp was replaced with an E.G.G FX-3A pulsed xenon lamp. A pulse generator indirectly triggered the lamp and advanced the channels of the signal averager. By adjusting the scan rate of the excitation spectrometer to the repetition rate of the flashlamp, almost any desired wavelength interval per memory channel could be obtained. The first 512 channels were used for storing the signal, while the other set of 512 channels stored the dark current and scattered light obtained from a second set of measurements. By subtracting the stored background from the stored signal it was possible to observe a very weak signal in the presence of a considerable amount of interference. The apparatus was also used to determine fluorescence decay times by keeping the fluorescence spectrometer fixed at a desired wavelength, and sweeping the channels with a predetermined time base.

Infrared transmission spectra were also measured on both Fe^{3+}-doped and undoped samples of $LiAl_5O_8$. The spectral range extended from 33 to 1000 cm^{-1}.

IV. EXPERIMENTAL RESULTS

A. Fluorescence Spectra of Ordered Phase

Figure 2 shows the ordered-phase fluorescence of $LiAl_5O_8$: Fe^{3+} at room temperature, 77, and 4.2 K. Pronounced changes in shape and in amplitude with temperature take place, although no very great changes in over-all width occur.

Considering first the 77-K spectrum, Fig. 2(b), we see a narrow line at 657 nm followed by broader and less distinct peaks at 666, 674, 685, and 697 nm.[10] The 657-nm line in this spectrum is identified later as an Fe^{3+} zero-phonon transition, the remaining peaks as vibronic sidebands. At 77 K, the zero-phonon line is barely resolvable into two components. The energy differences between the 657-nm line and the peaks of the four sidebands correspond to multiples (1, 2, 3, and 4) of 199 ± 12 cm^{-1}; see Table II.

Cooling to 4.2 K results in an appreciable narrowing of the 657-nm line to a width of about 0.0006 nm (16 cm^{-1}) and a concomitant increase in peak intensity. The two components of the 657-nm line seen at 77 K are now much better resolved. They are shown in the insert to Fig. 2(c). The appearance of the complex of sidebands changes little on cooling to 4.2 K.[11]

B. Excitation Spectra of Ordered Phase

Figure 3 shows the excitation spectrum of the 657-nm line at 77 K. From 370 to 680 nm, the 77-K spectrum resembles in most respects that seen

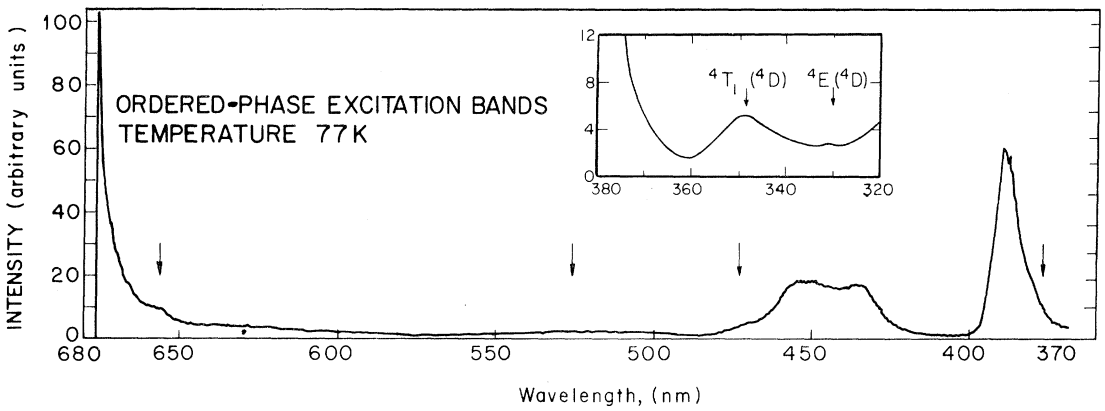

FIG. 3. Excitation spectrum of the fluorescence of ordered $LiAl_5O_8:Fe^{3+}$ at 77 K. The arrows indicate details which do not appear too clearly at room temperature, namely, slight shoulders at 370 and 475 nm, a weak line at 657 nm, and a more pronounced band at 520 nm. The insert shows the region below 380 nm.

at 300 K. The two prominent components of the 440-nm band are equally evident at 300 K, but the long-wavelength shoulder is not seen at room temperature. The broad 520-nm band is also somewhat more pronounced at 77 K. The 440- and 520-nm bands are better seen in Fig. 4. An almost completely obscured excitation line at 657 nm (shown by an arrow in Fig. 3) is shown more clearly in Fig. 5. The very strong charge-transfer band begins to appear at 360 nm at room temperature. Upon cooling at 77 K, this band shifts to below 305 nm, thereby exposing two weak bands at 349 and 330 nm. These are shown in the insert to Fig. 3.

In order to expose more clearly the 657-nm excitation line, the signal averaging referred to in Sec. III was employed. Moreover, the first sideband, rather than the 657-nm line itself, was monitored. Figure 5 shows the results obtained. A sharp line is seen in excitation at approximately 656 nm which, within the uncertainty of these measurements, corresponds to the position of the 657-nm line in fluorescence. (The resolution of the signal averager in these measurements was 2.5 nm per channel. The discrepancy of 1 nm between the peaks of the 657-nm line in excitation and fluorescence therefore is as good as can be expected.) Also seen in Fig. 5 is a broader band on the short-wavelength side of the 657-nm line.

TABLE II. Frequencies of the infrared-active modes of $LiAl_5O_8$, $LiFe_5O_8$, and of the $LiAl_5O_8:Fe^{3+}$ vibronic sidebands.

$LiAl_5O_8$		$LiFe_5O_8$		Fe^{3+} in $LiAl_5O_8$ vibronic
ordered	disordered	ordered	disordered	sidebands
865		706		851
771		667		
727	736	594	582	599
678		550		
640	645	471	470	
610		437		
556		396		
527	520	371	400	
484		358		361
440		332		
415	414	306		
394		249		
384		226		
354		202		
330		182		188

C. Far-Infrared-Transmission Spectra of Ordered Phase

Transmission spectra from 33 to 1000 cm^{-1} were obtained for $LiAl_5O_8$, for $LiAl_5O_8$ doped with 5-at.% Fe^{3+}, and for $LiFe_5O_8$. The spectrum of ordered $LiAl_5O_8$ consists of 15 narrow absorption lines extending from 865 to 330 cm^{-1}. No absorption is seen below 330 cm^{-1}. The spectrum of $LiFe_5O_8$ is similar except that the range of frequencies ex-

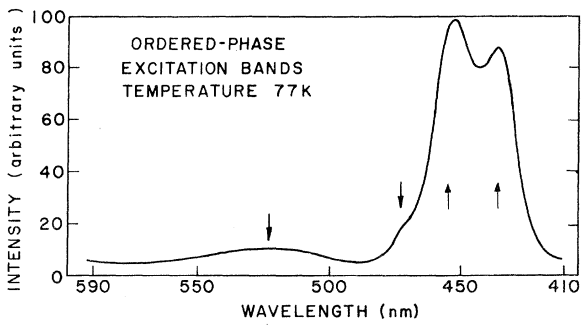

FIG. 4. A 77-K ordered-phase excitation spectrum similar to Fig. 3, but showing more clearly the splittings of the 450- and 529-nm bands.

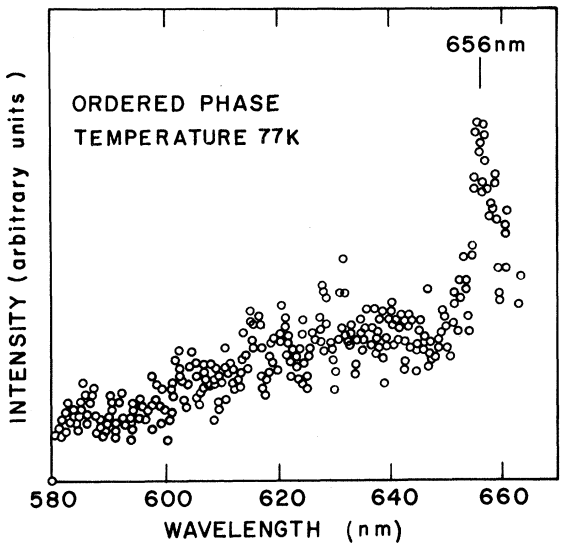

FIG. 5. Ordered-phase excitation spectrum taken at 77 K of the 666-nm vibronic sideband showing the zero-phonon absorption at 656-657 nm. Datat were obtained by means of a multichannel signal averager. Resolution is 2.5 nm per channel. The broad structure at the high-energy side is discussed in Sec. V A.

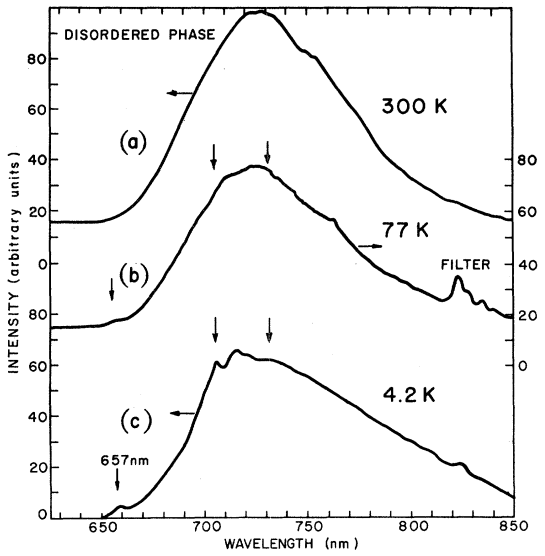

FIG. 6. Fluorescence of disordered $LiAl_5O_8:Fe^{3+}$ at (a) 300 K, (b) 77 K, and (c) 4.2 K. The position of the zero-phonon line in the *ordered* phase is shown by the arrow. The small peaks in the region of 825 nm are due to the fluorescence of a filter used to block the excitation radiation.

tends from 706 to 182 cm^{-1}. The vibrational frequencies of $LiAl_5O_8$ and $LiFe_5O_8$ are listed in Table II. Since our spectra are essentially identical with those recently obtained by DeAngelis and by others,[12,13] they are not shown here. We were unable to see any differences between the far-infrared spectra of pure $LiAl_5O_8$ and of Fe-doped $LiAl_5O_8$ which could be attributed to the presence of the Fe.

D. Fluorescence Spectra of Disordered Phase

Figure 6 shows the fluorescence of the disordered phase at 300, 77, and 4.2 K. The fluorescence, broad at room temperature, remains so at lower temperatures. Some semblance of structure is evident at 77 K as an irregularity near the peak of the band [(indicated by the arrow in Fig. 6(b)]. This irregularity is also seen at 4.2 K. The 77- and 4.2-K spectra are indicative of inhomogeneous broadening. Also seen in Figs. 6(b) and 6(c) is a trace of a peak at 657 nm, the wavelength corresponding to the sharp line in the ordered phase. If this peak is due to some residual ordered-phase component, its concentration is at most 0.1% of the total Fe^{3+} present in the sample.

E. Excitation Spectra of Disordered Phase

The excitation spectrum at 77 K of the disordered-phase fluorescence is shown in Fig. 7. The general appearance is similar to the room-temperature spectrum,[2] except for a broad weak band at about 550 nm which was not seen previously. This band is shown more clearly in Fig. 8; it corresponds to the 520-nm band seen in the ordered phase. The position of this band in the disordered-phase spectrum is consistent with its assignment to the $^6A_1(^6S) \rightarrow {}^4T_1({}^4G)$ transition.

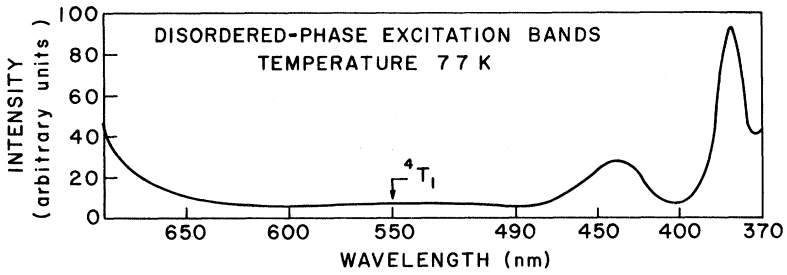

FIG. 7. Excitation spectrum of the fluorescence of the disordered $LiAl_5O_8:Fe^{3+}$ phase at 77 K. Note the broad band at 550 nm labeled $^4T_1$.

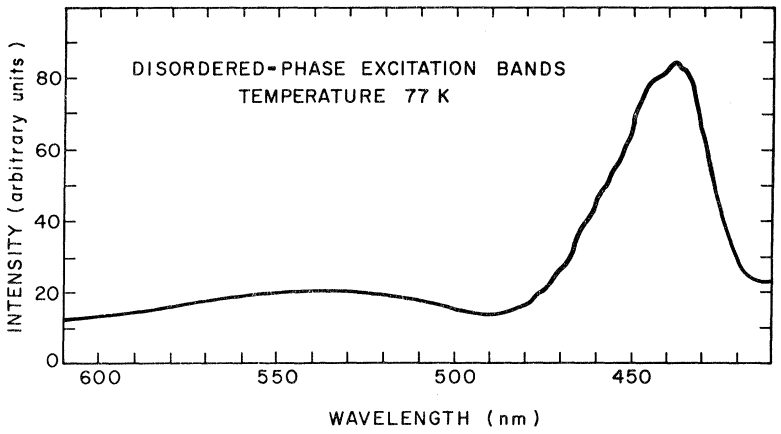

FIG. 8. 77-K excitation spectrum of the disordered phase, similar to Fig. 7, but showing more clearly the 440- and 550-nm bands.

V. DISCUSSION

A. Low-Temperature Fluorescence Spectra of Ordered Phase

The most striking feature of the low-temperature luminescent properties of Fe^{3+} in $LiAl_5O_8$ is the sharp 657-nm fluorescence line. The evidence for this being a zero-phonon transition is fairly direct. First, this line is very narrow in comparison to the room-temperature fluorescence. More importantly, it is seen at the same wavelength both in fluorescence and in excitation. The latter constitutes the most important single piece of evidence for a "zero-phonon" transition. Finally, elementary considerations indicate that the zero-phonon line should be the highest-energy transition in fluorescence emission and the lowest energy in fluorescence excitation. This can be verified from examination of Figs. 2 and 5, respectively.

As can be seen in Figs. 2(b) and 2(c), the zero-phonon line consists of two components. The widths and relative intensities of these components vary with temperature, but their separation, approximately 7–7.5 Å (16–18 cm^{-1}) remains fixed between 77 and 4.2 K. The most likely explanation of this 16-cm^{-1} splitting attributes it to spin-orbit splitting of the $^4A_2$ component of the $^4T_1$ state of Fe^{3+}.[14] (The band assignments will be discussed later.) The intensity ratio of the two components of the zero-phonon line is approximately 0.8 at 77 K and 0.3 at 4.2 K. Since thermal equilibrium between two such closely lying levels should take place in less than the approximately 10^{-2}-sec radiative lifetime for the $^4T_1 \rightarrow {}^6A_1$ transition, these intensity ratios reflect the local temperature of the excited radiating centers. At 77 K, the local temperature is close to the bath temperature. At 4.2 K, the local temperature is 18 K. Such a high local temperature implies a very weak coupling between the radiating center and the lattice.

The over-all width of the zero-phonon line at 77 K is approximately 35 Å (81 cm^{-1}). Allowance for the 7.5-Å separation between the components to this line reduces the individual component width to approximately 27 Å (62 cm^{-1}). At 4.2 K, the width of each component is approximately 7 Å. One should note, however, that the spectrometer resolution at which the measurements were made is close to 7 Å.

Turning to the fluorescence sidebands, two features are evident. The frequency interval between the sideband peaks is nearly constant (199 ± 12 cm^{-1}) and well below the lowest infrared lattice mode of $LiAl_5O_8$ (see Table II); it is close to the 182-cm^{-1} mode of $LiFe_5O_8$. The 77-K fluorescence decay time measured at the 685-nm peak is quite long (8.6 msec), and is the same as that measured at the zero-phonon line. This indicates that both the sidebands and the zero-phonon line have a common origin. The observed common frequency interval and the well-defined structure suggest that the sidebands correspond to local modes of vibration of an FeO_4 center rather than to lattice modes.[15] The long decay times, the small temperature dependence of the decay time (6.2 msec at room temperature), and the presence of local modes and of a zero-phonon line,[16] are all consistent with a weak-lattice-impurity coupling.

A weak vibronic coupling of the luminescent center to the lattice does not contradict our other evidence of a strong bond between the Fe^{3+} and its neighboring oxygen ligands deduced from Stokes shift and covalency affects. The former depends on the coupling of the FeO_4 tetrahedra to the lattice, while the latter depends on strength of the Fe-O bonds within the tetrahedron.

The sidebands seen in the excitation spectrum, Fig. 5, reflect the vibrational structure of the excited state. The absence of well-defined structure here makes analysis less certain.

B. Low-Temperature Fluorescence Spectra of Disordered Phase

Just as the zero-phonon line is the most con-

spicuous feature of the low-temperature fluorescence of the ordered phase, its absence is the most notable feature of the disordered phase. The most important characteristics of the disordered-phase fluorescence are (i) a relatively broad band, 1600 cm^{-1} in width at room temperature. (ii) A width which is only slightly sensitive to temperature. Cooling to 77 K reduces the width to 1530 cm^{-1}; essentially all the reduction occurs on the low-energy side. Further cooling to 4.2 K does not cause any additional width reduction. (iii) A variation in decay time in different regions of the emission band.

Although no zero-phonon line is present, some structure can be seen in the fluorescence band. A characteristic irregularity near the peak is more pronounced at 77 and 4.2 K but can be seen even at room temperature. The characteristics of the fluorescence of the disordered phase suggest it to be inhomogeneous in nature. Such a situation can result from site distortions due to local strains. These could be brought about by the very rapid thermal quenching required to prepare the specimen. The inhomogeneous nature of these optical spectra is in accord with Folen's electron-spin-resonance measurements[9] which indicated a distribution of spin-Hamiltonian parameters in the disordered phase.

C. Site Occupancy

In MVAB-I we presented evidence which indicated quite strongly that the fluorescent properties of the ordered phase of $LiAl_5O_8:Fe^{3+}$ are due to Fe^{3+} ions situated at tetrahedral sites, while the fluorescent properties of the disordered phase are associated with Fe^{3+} at octahedral sites. The low-temperature measurements presented here tend to confirm these site assignments. The most significant evidence is the presence of the zero-phonon line in the ordered phase, and its absence in the disordered phase.

Electric-dipole transitions to or from the ground state for d^5 ions situated in crystalline environments are normally both spin and parity forbidden. Configurations of opposite parity, however, can be mixed in by odd components of the crystal field. Thus, ions situated at sites lacking inversion symmetry generally exhibit considerably stronger optical transitions than those at centrosymmetric octahedrally coordinated sites. Interaction with lattice vibrations provides another mechanism of overcoming parity restriction. However, the very nature of the zero-phonon line makes such phonon assistance inoperative. Hence the zero-phonon line would be strictly forbidden in a centrosymmetric octahedral environment, but should be partially allowed in a tetrahedral environment. This leads to the generalization that electric dipole zero-phonon transitions should be more intense for ions located at tetrahedrally coordinated sites than for those at octahedrally coordinated sites. It supports our assignments of the Fe^{3+} sites in the two phases.

D. Crystal Field Parameters

In Sec. 4.2 of MVAB-I, we described the method used to fit the crystal field parameters to the measured band positions. It involved finding the best values of B, C, and Dq from a three-parameter least-squares fit. Due to the failure at room temperature to observe a band near 520 nm, some ambiguity existed in the level assignments of the disordered phase. Neither the introduction of the Trees correction nor of "covalency" succeeded in resolving the problem. We do now observe this band at 554 nm in the disordered phase at 77 K. This removes the ambiguity in the room-temperature data; we now have an excellent fit between theory and observation for both the ordered and disordered phases. The fit requires that the $^6A_1(^6S) \rightarrow {}^4T_1(^4G)$ transition of Fe^{3+} undergo a rather large Stokes shift, amounting to 4400 cm^{-1}. The three-parameter fit is sufficiently good, moreover, to leave nothing to be gained from the use of a covalency correction. The values of B, C, and Dq and observed and calculated energy levels are given in Table III.

At this point, it is worth commenting on the effect a large Stokes shift has on the observed and calculated energies of the excited states of Fe^{3+}.

TABLE III. Transition energies in $LiAl_5O_8:Fe^2$ calculated for various crystal field parameter sets. Observed values are listed for comparison.

	Ordered phase			
	300 K		77K	
	$B = 626.4$ cm^{-1}		$B = 638.4$ cm^{-1}	
	$C = 3875.4$ cm^{-1}		$C = 3868$ cm^{-1}	
	$Dq = 940.4$ cm^{-1}		$Dq = 951.9$ cm^{-1}	
Transition	Calculated (cm^{-1})	Observed (cm^{-1})	Calculated (cm^{-1})	Observed (cm^{-1})
$^6A_1(^6S) \rightarrow {}^4T_1(^4G)$	19123	19120	19084	19084
$^6A_1(^6S) \rightarrow {}^4T_2(^4G)$	22437	22434	22472	22472
$^6A_1(^6S) \rightarrow \left\{{}^4A_1(^4G) \atop {}^4E\right.$	25641	25641	25724	25723
$^6A_1(^6S) \rightarrow {}^2T_2(^2I)$	25703		25596	
$^6A_1(^6S) \rightarrow {}^4T_2(^4D)$	28193		28328	28670
$^6A_1(^6S) \rightarrow {}^4E(^4D)$	30025		30193	30340
$^6A_1(^6S) \rightarrow {}^2A_2(^2I)$	31957		31935	
$^6A_1(^6S) \rightarrow {}^2T_1(^2I)$	32086		32069	
	Disordered phase			
	300 K		77 K	
			$B = 854.0$ cm^{-1}	
			$C = 3448.2$ cm^{-1}	
			$Dq = 1019.9$ cm^{-1}	
Transition	Calculated[a]	Observed (cm^{-1})	Calculated (cm^{-1})	Observed (cm^{-1})
$^6A_1(^6S) \rightarrow {}^4T_1(^4G)$			18051	18051
$^6A_1(^6S) \rightarrow {}^4T_2(^4G)$		22589	22573	22573
$^6A_1(^6S) \rightarrow \left\{{}^4A_1(^4G) \atop {}^4E\right.$		25570	25783	25783

[a]Not fitted due to insufficient data.

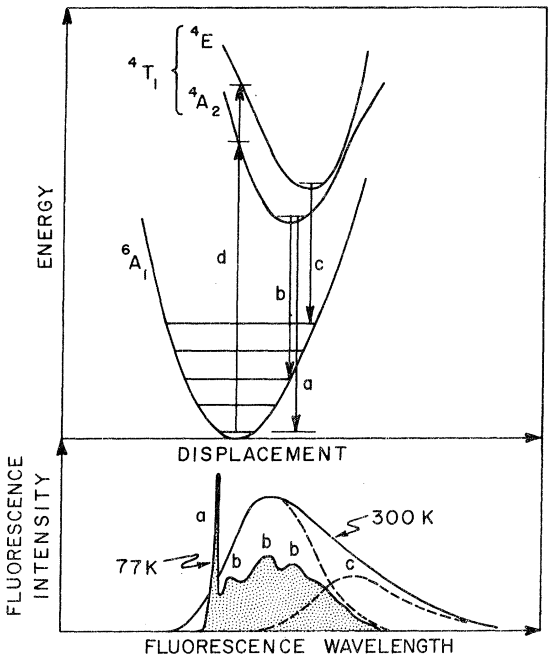

FIG. 9. Configurational coordinate representation of the fluorescence at 300 and 77 K. The zero-phonon transition is labeled *a*; typical vibronic transitions are shown, labeled *b*; a transition from the upper ^4E component of the excited state is labeled *c*. The contributions of these transitions to the fluorescence are shown in the lower portion of the figure, the shaded area being the 77-K fluorescence, and the dashed curves representing the components of the 300-K fluorescence.

The common method of specifying energies of electronic states, as in Table III, ignores the effects of lattice vibrations. Such energies therefore may or may not correspond to the loci of the minima of the potential wells which characterize these states. However, when a large Stokes shift is present, optical transitions do not in general occur between these potential minima. Instead, in keeping with the Franck-Condon approximation, they will occur vertically, without any change in configuration coordinates[17] (see Fig. 9). Consequently, optical excitation or absorption transitions are likely to overestimate the separation between states as defined by their minima, while fluorescence transitions are likely to underestimate them. Where splittings are present as in the $^4T_1$ and $^4T_2$ manifolds, the occurrence of a Stokes shift can not only produce somewhat erroneous values for these splittings, but can also indirectly introduce apparent temperature variations in the magnitudes of these splittings. These apparent variations can result from even very small shifts in the barycenters of optical bands having temperature-dependent linewidths, as in the case of the $^4T_2$ band described below.

The magnitude of the Stokes shift in this material appears to be larger than one usually observes in transition-metal ions. In calculating the values of *B*, *C*, and *Dq* of Table III, and in determining the best fit to the observed data, only optical transitions to the ^4G-derived states were used. The energies of these transitions were obtained from optical-excitation data alone and not from emission, and may therefore be presumed to take place vertically from the ground state to vibrationally excited levels of the upper state. Since the ligand-field theory used for our calculations assumes the same configuration coordinates for all of the energy levels at a given *Dq*, the method of taking our measurements is in accord with the requirements of the theory. The excellent agreement we obtain between our calculated and observed energy-level values is therefore sufficient justification for the presence of such a large Stokes shift.

E. Crystal Field Splittings

EPR and our ME data indicate that the ground state of the Fe^{3+} ion is at a site having axial (trigonal) symmetry. A trigonal crystal field would separate the $^4T_1(^4G)$ and $^4T_2(^4G)$ triplets into their component $^4A_2, ^4E$ states and $^4A_1, ^4E$ states, respectively. The presence of splittings can be seen in the room-temperature fluorescence of the ordered phase[2] and in the excitation spectra of the ordered phase at both 300 and 77 K. From the measured excitation data, the separation of the components of the $^4T_1$ and $^2T_2$ bands at 300 K are $^4T_1$, 680 cm^{-1}; $^4T_2$, (690 ± 42) cm^{-1}. At 77 K the $^4T_2$ components appear to be separated by 830 cm^{-1}. These values do not represent the crystal field splittings as defined by the potential minima for the reasons discussed in Sec. V D. What appears to be a relatively large temperature-dependent $^4T_2$ splitting is due mainly to very small variations in the maxima of the optical-excitation bands.

We estimate the energy separation of the components of the $^4T_1$ state in terms of a particular model. We assume that a trigonal distortion makes the $^4A_2$ the lower component level as shown in Fig. 9, and that the level populations of the $^4A_2$ and ^4E components are in thermal equilibrium. If the latter assumption were pure, the ratio of the lifetimes of the two levels would be slightly different. Let $I(^4A_2)$ and $I(^4E)$ represent the integrated intensities of the $^4A_2 \rightarrow {}^6A_1$ (668 nm) and $^4E \rightarrow {}^6A_1$ (697 nm) transitions, respectively. Then

$$\frac{I(^4E)}{I(^4A_2)} = \frac{n(^4E)/\tau_{697}}{n(^4A_2)/\tau_{668}},$$

where *n* refers to the steady-state population of the indicated level, and τ is the measured radiative lifetime. In thermal equilibrium

TABLE IV. $^4T_1$ splitting Δ derived from fluorescence data.

T (K)	$I(^4E)/I(^4A_2)$	Δ/kT	Δ (cm^{-1})
297	0.54	2.69	560
338	0.59	2.59	608

$$n(^4E)/n(^4A_2) = 2e^{-\Delta/kT},$$

where the factor 2 takes into account the multiplicities of the states involved and Δ is their energy separation.

The integrated intensities of the two components of the room-temperature fluorescence were determined by means of a duPont curve resolver. The τ's had been measured previously at 297 K. The ratios of $I(^4E)$ to $I(^4A_2)$ at two temperatures and the values of Δ so derived are presented in Table IV. In view of the absence of strict thermal equilibrium, the Δ values obtained in this manner are very approximate.

A field that splits $^4T_1(^4G)$ should also split the $^4T_2(^4G)$ state except that in the latter the ^4E should be the lower level on the basis of our assumption. The data on the $^4T_2$ spectrum are derived from excitation measurements, which are related to absorption processes. From the degeneracy of the levels, we therefore expect the ^4E component to have about twice the excitation strength of the $^4A_1$. Figure 3 indicates that the lower-frequency band of the $^6A_1(^6S) \rightarrow {}^4T_2(^4G)$ doublet does in fact have twice as great an integrated intensity as the higher one, consistent with the above analysis. However, the assumption of a trigonal field for the excited states provides no explanation for the very weak third component of this manifold. This consists of a shoulder at about 480 nm and contributes a few percent to the total strength of the transition.

The basis for assuming an axial field in the above estimates of crystal field splittings is the result of both our ME[1] measurements and of EPR measurements.[9] These measurements indicate that both the A sites in the ordered phase and the B sites in the disordered phase have axially symmetric electric field gradients (EFG) at the Fe^{3+} positions. The trigonal component of the A sites of the ordered phase is well defined, and is formally associated with the disposition of the Li ions; see Table I. The local symmetry of the B site in the disordered phase is more obscure inasmuch as it cannot be inferred from the average disordered-state symmetry listed in Table I.

If we apply the trigonal distortion we see in our ME measurements to the $^4T_1(^4G)$ and $^4T_2(^4G)$ states, we expect to see each of these states split into two components. This is in general agreement with our observations, except for the third $^4T_2$ component noted earlier. Such a direct application of our ME results is open to serious question, however. First, the $^6A_1$ ground state is spherically symmetric and remains essentially so in the ME transitions. The optical splittings are those of the nonspherically symmetric components of the ^4G state. Therefore our ME results are applicable only if we assume that the symmetry properties of the impurity site are independent of the electronic configuration of the impurity. Second, the ordering of the $^4T_1$ components which we have deduced from our optical measurements is not consistent with the ordering which we calculate from our ME results using a simple point-charge model. The hyperfine-field properties of the $^6A_1$ Kramers doublet derived from our ME studies show these states to have a moderate degree of ionicity which provides some justification to the use of a point-charge model. Using this model, we correlated the EFG value observed by ME with the trigonal-field splitting of the $^4T_1$ components. We obtained the correct magnitude of the calculated splittings, but the reverse ordering of the components. Any attempt to calculate such splittings from first principles is complicated further by the disparity in size between the Fe^{3+} and the Al^{3+} ions.

Rather than attempt a direct correlation between the ME and optical results, a more reasonable explanation rests on the assumption of a Ham[17] effect. The presence of a third component in the $^4T_2(^4G)$ excitation bands of the ordered phase implies an A-site symmetry lower than trigonal. This could be produced in the $^4T_2$ state by a Jahn-Teller distortion modified by intermediate spin-orbit coupling.[18] In such an interpretation the components of the $^4T_2$ states can no longer be designated as simply ^4E and $^4A_1$ states.[19] The presence of this Ham effect can also be used to account for the magnitude of the splitting seen in the zero-phonon line.[20]

Although most of these same considerations would apply to the disordered-phase spectra, the effects of disordering make interpretation difficult.

VI. CONCLUSIONS

Figure 9 summarizes the major features of the low-temperature fluorescence of ordered $LiAl_5O_8$: Fe^{3+}. The ground state is designated as $^6A_1$ in standard notation. Assuming a trigonal field for simplicity, the first excited state $^4T_1$ would be split into a doubly degenerate ^4E level and a singly degenerate $^4A_2$ level by the action of the trigonal component of the "crystal field" potential. The $^4A_2$ component is the lower.

In accord with our measurements, the vibrational levels of the $^6A_1$ state are depicted as occurring at intervals of 199 cm^{-1}. The zero-phonon line, labeled a, corresponds to emission from the lowest $^4A_2$ vibrational state to the lowest $^6A_1$ vibrational level.

This transition is shown as terminating at a point which lies outside the normal $^6A_1$ configuration-coordinate "space." Typical transitions from the lowest $^4A_2$ vibrational level to some of the $^6A_1$ vibrational levels are shown, labeled *b*. Such transitions account for the vibrational account for the vibrational sidebands seen at 4 and 77 K.

Excitation from the ground state to the $^4A_2(^4T_1)$ components is indicated by lines *d*. While two excitation bands should be seen, they apparently merge into one experimentally. A large Stokes shift (approximately 30%) ensues. We attribute this magnitude to the steepness of the energy-configuration-coordinate curves which result from the strong bonding between the central Fe^{3+} ion and its ligands, thus creating a relatively stiff complex. In such a case, even a relatively small difference in the lattice equilibrium coordinates of the ground and excited electronic states can give rise to a large difference between corresponding energies as measured in excitation and emission.

As the temperature is raised from 77K, there is an increase in the number of phonons available at the impurity centers, as well as an increase in the coupling of the impurity center to the lattice modes. The result is an increase in the probabilities for the vibronic transitions at the expense of the zero-phonon line, as well as a loss of the details of the individual vibronic transitions. At room temperature, this leads to the production of a broad smooth emission band with the complete elimination of the zero-phonon line.[15] In addition, the relative contribution of the upper $^4E(^4T_1)$ metastable level to the emission becomes greater, leading to a more pronounced appearance of a two-component fluorescence. These consequences are shown schematically in Fig. 9, where the shape of the fluorescence at 300 K is placed in relation to the 77-K emission.

Finally, we wish to relate some of the above conclusions with those derived from ME studies which were conducted concurrently on many of the same $LiAl_5O_8:Fe^{3+}$ samples. The interpretation of the ME results in ordered $LiAl_5O_8:Fe^{3+}$ was in accord with tetrahedral-site occupancy by the Fe^{3+} ion, with earlier EPR spectra, and with our optical observation of a zero-phonon transition. The ME resonances were characterized by unusually long spin-lattice relaxation times. We can attribute these to a relatively weak phonon–Fe^{3+}-ion interaction. A similar interpretation is suggested by the presence of local modes in the fluorescence vibronic spectra. Examination of the ME data revealed that the resonance amplitudes increased by approximately 12% when the temperature was lowered from 300 to 4.2 K. Such a relatively small enhancement is in accord with the notion of strong Fe-O bonds. This again is consistent with our interpretation of the fluorescence spectrum. However, the algebraic sign of the nuclear-electric-quadrupole splitting seen by ME does not correspond, on the basis of a simple point-charge model, to the sense of the ordering of the split optical bands deduced independently. Most likely the Jahn-Teller and Ham effects are operative in the excited optical states.

The ME results for disordered (high-temperature) phase $LiAl_5O_8:Fe^{3+}$ were not as informative. The resonances were very broad. In spite of the difficulties in analyzing these spectra the following conclusions were drawn: (a) The symmetry of the Fe^{3+} site is lower than cubic; (b) the phonon–Fe^{3+}-ion interaction is relatively weak at room temperature.

The over-all picture emerges of an Fe^{3+} ion strongly bound to its neighboring ions to form FeO_4 and FeO_6 complexes which are loosely coupled to the lattice. The Fe^{3+} fluorescence is dominated by local modes rather than by impurity-lattice interaction, probably even at or close to room temperature.

ACKNOWLEDGMENTS

We wish to thank Dr. W. D. Partlow of the Westinghouse Research Laboratories for measurements at 4.2 K, Dr. F. M. Ryan for the measurements with cathode-ray excitation, and R. J. Perevuznik for assisting with some of the measurements at 77 K. We wish to thank Professor W. G. Fateley of Carnegie-Mellon University for allowing us the use of his infrared facilities, and Dr. P. M. Jaffe of Zenith Radio Corp. for supplying us with one of his phosphor samples for comparison. We also wish to thank Dr. J. Murphy of the Westinghouse Research Laboratories for various comments and discussions.

---

†Based in part on a dissertation submitted by P. J. Viccaro to the Physics Department, Carnegie-Mellon University, in partial fulfillment of the requirements for the Ph.D. degree.

*Supported in part by the Office of Naval Research and the National Science Foundation.

‡N.D.E.A. Fellow. Present address: Instituto de Física, Universidade Federal do Rio Grande do Sul, Porto Alegre, Brasil.

§Also Department of Electrical Engineering, Carnegie-Mellon University.

[1]P. J. Viccaro, F. de S. Barros, and W. T. Oosterhuis, Phys. Rev. B (to be published).

[2]N. T. Melamed, P. J. Viccaro, J. O. Artman, and F. de S. Barros, J. Luminescence 1-2, 348 (1970).

[3]E. W. Gorter, Philips Res. Rept. 9, 295 (1954); 9, 321 (1954); 9, 403 (1954); P. B. Braun, Nature 170, 1123 (1952); R. W. G. Wyckoff, *Crystal Structures*, 2nd

ed. (Interscience, New York, 1965), Vol. III, p. 75.

[4]R. K. Datta and Rustrum Roy, J. Am. Ceramic Soc. 46, 388 (1963); R. K. Datta, Ph.D. thesis (Pennsylvania State University, 1961) (unpublished).

[5]E. Kato, Bull. Chem. Soc. (Japan) 32, 585 (1959).

[6]E. J. Verwey and E. L. Heilman, J. Chem. Phys. 15, 174 (1947).

[7]Arthur Miller, J. Appl. Phys. 30, 24S (1959).

[8]J. A. Schulkes and G. Blasse, J. Phys. Chem. Solids 24, 1651 (1963).

[9]V. J. Folen, J. Appl. Phys. 33, 1084 (1962); V. J. Folen, *Proceedings of the First International Conference on Paramagnetic Resonance*, edited by W. Low (Academic, New York, 1963), p. 68.

[10]A small peak at 712.5 nm is attributed to Cr^{3+} present as an impurity. It is not always seen in our samples, and has a significantly different excitation spectrum from that of Fe^{3+}. The fluorescence of Cr^{3+} in $LiAl_5O_8$ has recently been reported [M. P. Pietrow, R. Wadas, and W. Wardzinsky, J. Phys. (Paris) Suppl. 27, C1 (1971)]. The position and shape of the reported emission agree with our observation.

[11]A blue fluorescence has been reported by Jaffe in $LiAl_5O_8:Fe^{3+}$ [P. M. Jaffe, J. Electrochem. Soc. 115, 1203 (1968)]. It appears only under cathode-ray excitation. We have repeated his measurements with similar results. This fluorescence could result from a $^4T_2(^4G) \rightarrow {}^6A_1$ transition (see Sec. V).

[12]W. B. White and B. A. De Angelis, Spectrochimica Acta 23A, 985 (1967); B. A. De Angelis, Ph.D. thesis (Pennsylvania State University, 1969) (unpublished).

[13]Pierre Tarte, Compt. Rend. 254, 2008 (1962); S. Hafner and F. Laves, Z. Krist. 115, 321 (1961).

[14]The more usual causes of zero-phonon line structure appear to be local strains which result in a distribution of zero-phonon frequencies [see D. B. Fitchen, *Physics of Color Centers*, edited by W. Beall Fowler (Academic, New York, (1968)]. This is evidently not the case here.

[15]M. V. Klein, in Ref. 14, p. 429; C. B. Pierce, Phys. Rev. 135, A83 (1964).

[16]D. E. McCumber, Phys. Rev. 135, A1676 (1964).

[17]M. D. Sturge, in *Solid State Physics*, edited by F. Seitz, D. Turnbull, and H. Ehrenreich (Academic, New York, 1967), Vol. 20, p. 91.

[18]F. S. Ham, in *Electron Paramagnetic Resonance*, edited by S. Geschwind (Plenum, New York, 1971).

[19]F. S. Ham, in *Optical Properties of Ions in Crystals*, edited by H. M. Crosswhite and H. W. Moos (Interscience, New York, 1967), p. 357.

[20]We are indebted to Professor D. S. McClure for pointing this out to us.

PHYSICAL REVIEW B VOLUME 5, NUMBER 9 1 MAY 1972

Electron-Nuclear Double Resonance of Samarium 147 and Samarium 149 Tripositive Ions in Lanthanum Trichloride Single Crystals *†

I. Y. Chan‡ and Clyde A. Hutchison Jr.
Department of Chemistry and Enrico Fermi Institute, The University of Chicago, Chicago, Illinois 60637
(Received 30 August 1971)

The electron-nuclear-double-resonance spectral frequencies of $^{147}Sm^{+3}$ and $^{149}Sm^{+3}$ ions dilutely substituted at La^{+3} ion sites in $LaCl_3$ single crystals at 2.07 °K have been measured. The experimental results for both nuclides have been summarized by giving values of the parameters in a spin Hamiltonian for a least-squares best fit to the measurements. The values of (a) nuclear g factors and nuclear magnetic-dipole moments for both nuclides, of (b) $\langle r^{-3} \rangle$ for the f electron-nuclear distance in Sm^{+3}, of (c) ratios of nuclear magnetic-dipole moments and (d) ratios of nuclear electric-quadrupole moments for the two nuclides, and of (e) the ratio of the crystal-field shielding and antishielding factors $1-\sigma_2$ and $1-\gamma_\infty$ for Sm^{+3} in $LaCl_2$, which are obtainable from these measurements, are discussed and tabulated.

I. INTRODUCTION

In previous work[1,2] in this laboratory the electron-nuclear-double-resonance (ENDOR) spectra of $^{143}Nd^{+3}$ and $^{145}Nd^{+3}$ ions, with electron configuration f^3 in $LaCl_3$ single crystals, were studied. These investigations afforded detailed information on the f electron states and values of $\langle r^{-3} \rangle$, and they permitted the obtaining of accurate values of the magnetic-dipole moments ($M1$) of the nuclei ^{143}Nd and ^{145}Nd, and of the ratio of electric-quadrupole moments ($E2$) of these two nuclides.

In this present work we have made similar ENDOR studies of $^{147}Sm^{+3}$ and $^{149}Sm^{+3}$ ions, with electron configuration f^5, in single crystals of $LaCl_3$. The electron-paramagnetic-resonance (EPR) spectra of these ions in $LaCl_3$ crystals have been analyzed in previous work[3] in this laboratory. The structure of the $LaCl_3$ crystal has been determined by x-ray diffraction by Zachariasen.[4] The optical spectra of Sm^{+3} in $LaCl_3$ single crystals have been studied by Dieke and his co-workers[5,6] and by Hadni and Strimer.[7] Wybourne[8] has provided a theoretical analysis of the electronic states of ions with configuration f^5 in such crystals. Freeman and Watson[9] have discussed the application of approximate